Possibility of M_w 9.0 mainshock triggered by diffusional propagation of after-slip from M_w 7.3 foreshock

Ryosuke Ando and Kazutoshi Imanishi

Geological Survey of Japan, National Institute of Advanced Industrial Science and Technology, Cetral 7, 1-1-1 Higashi, Tsukuba, Ibaraki 305-8567, Japan

(Received April 7, 2011; Revised May 17, 2011; Accepted May 18, 2011; Online published September 27, 2011)

For the 2011 off the Pacific coast of Tohoku, Japan, Earthquake, we have investigated the spatio-temporal changes in seismicity from the M_w 7.3 foreshock, March 9, 2011, 11:45, to the M_w 9.0 mainshock, March 11, 14:46 (Japan Standard Time). We found that seismic activities slowly migrated from the source area of the foreshock, which presumably reflected the propagation of the after-slip. The mainshock rupture was initiated when the migration reached the hypocentral location of the mainshock. We also found that the migration slowed down as it expanded, where the migration distance was well fitted by a certain curve proportional to the square root of the duration, suggesting that the propagation was limited by diffusion with a diffusion coefficient of about 10^4 m^2 s^{-1}. This slow slip mechanism differs from nucleation-related pre-slip traditionally applied in earthquake predictions. The obtained value of the diffusion coefficient is of the same order of magnitude as that reported for the migration of a deep non-volcanic tremor. These results appear to be compatible with a conceptual model having strongly coupled patches which, although being separated by decoupled stable regions on this plate-interface, are not mechanically isolated and which became interactive when they broke.

Key words: Tohoku Earthquake, foreshock, triggering, after-slip, diffusion.

1. Introduction

The mainshock of the 2011 off the Pacific coast of Tohoku Earthquake broke the plate interface over almost 500 km (Fig. 1, inset) resulting in a moment magnitude of M_w 9.0. The sole M 7-class earthquake on the plate interface occurred just before the mainshock, about 1.8×10^5 seconds (51 hours) earlier, about 40 km away up-dip (hereafter, we call this event simply the foreshock). The extent of the foreshock focal area is thus much constrained by the spatial distribution of its immediate aftershocks (Fig. 1) and a seismic inversion (Hayes, 2011). Although any conclusions derived from such different datasets is uncertain, it is indicated that the rupture was initiated at the southern end of the source area and the coseismic rupture mainly propagated towards the north. According to a back-projection analysis, the rupture area of the mainshock was partitioned from, and did not overlap with, the foreshock area (Kiser and Ishii, 2011).

Aseismic after-slip is often observed associated with large earthquakes showing a complementary spatial distribution to coseismic slip areas (e.g., Yagi and Kikuchi, 2003; Miyazaki *et al*., 2004). In general, after-slip, aftershocks and along-fault migrations of large earthquakes have been described by diffusional processes, which are considered in relation to fault zone rheology (e.g., Savage, 1971; Ida, 1974) together with contributions from viscous mantle rebound which has an affect for much longer periods: a few years (e.g., Lehner *et al*., 1981). More recently, it is proposed that a slow earthquake family may be governed by diffusion (Ide *et al*., 2007; Ide, 2010; Ando *et al*., 2010; Nakata *et al*., 2011), with the migration fronts of tremor and slow slip events (SSEs) following parabolic curves,

$$T = (1/D)L^2, \tag{1}$$

where T and L denote the duration and distance of the migration, respectively, and the constant D is called the diffusion coefficient presuming underlying diffusional processes. In particular, Ide (2010) found that $D \sim 10^4$ m^2 s^{-1} explained the data well by analyzing tremor migration beneath western Shikoku for the Nankai subduction zone.

Foreshock-mainshock sequences are also recognized as earthquake doublets, observed in various tectonic settings, which phenomenon has been understood in terms of defined fault segmentations in some form (e.g., Lay and Kanamori, 1980; Engdahl *et al*., 2007; Nakano *et al*., 2010). They serve as a type of earthquake triggering and stress transfer (King *et al*., 1994; Gomberg *et al*., 2001). This context has particular importance in understanding the current sequence of events, because it has been believed that the plate-interface below the Japan trench contains strongly-coupled patches that are relatively small, and which define strong segmentations as impeding gigantic earthquakes (e.g., Lay and Kanamori, 1981). But, on this occasion, is this view totally wrong? In this paper, we reexamine it in the light of the currently observed foreshock-mainshock sequence.

We concentrate on the data analysis for the 2011 Tohoku Earthquake to clarify the seismicity migration pattern

doi:10.5047/eps.2011.05.016

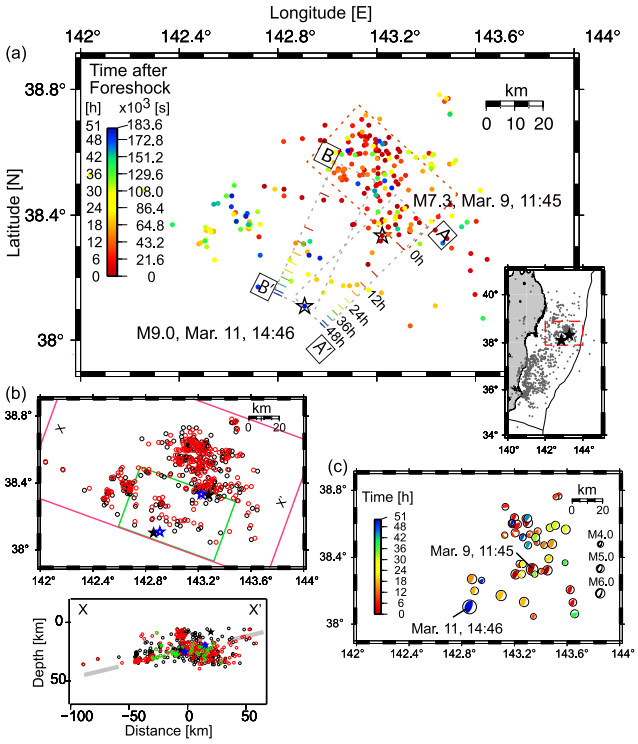

Fig. 1. Distribution of earthquake events between foreshock and mainshock. (a) Filled circles denote the epicenters of the earthquakes and their colors represent elapsed time from the foreshock as shown by the color bar scale. Stars indicate the epicenters of the foreshock and the mainshock. The red dotted rectangle very roughly encloses the foreshock focal area. Seismicity is sampled for Fig. 2 from two gray dotted rectangle areas; the colored tick marks inside them represent calculated rupture front locations at each elapsed time shown by the colors assuming the diffusion coefficient $D = 0.78 \times 10^4$ (refer to the text for the detail). (Inset) Mainshock focal area with seismicity from March 9 to 13, 2011 (gray dots). The area enclosed by a red rectangle is magnified. (b, upper) Map view showing relocated hypocenters (red circles) and initial hypocenters determined by JMA (black circles). The blue and black stars are hypocenters of the foreshock and the mainshock, respectively, after and before the relocation. (b, lower) Vertical cross-sectional view of the upper panel along X–X′. Green circles denote hypocenters in a green rectangle in (b, upper). (c) CMT (Centroid Moment Tensor) solutions colored with time after the foreshock.

which began at the foreshock and lasted until the mainshock. The background seismicity is also reviewed. An intuitive understanding of the physical background will be given by a model having brittle-ductile mixed fault heterogeneity (Ando *et al.*, 2010; Nakata *et al.*, 2011). We will see below that the seismicity migration follows well the above-mentioned parabolic pattern and that the onset timing of the mainshock corresponds to the arrival of the migration front to the mainshock hypocentral location.

2. Method

In order to obtain the seismic activity data, we have applied the double-difference earthquake location algorithm of Waldhauser and Ellsworth (2000) to routinely determined P- and S-phase arrival time readings from the Japan Meteorological Agency (JMA). Each event is linked to its neighbors through commonly observed phases, with the average distance between linked events being 20 km. The data was obtained from the Japanese nationwide seismic network and the readings by JMA were obtained during the period between the foreshock and the mainshock. We applied a bootstrap resampling technique to quantify the precision of a given location (see Waldhauser and Ellsworth, 2000); we obtained relative location errors, defined as 1σ, of about 2 km in both horizontal and vertical directions, which is sufficient to discuss the relative locations of the earthquakes during the migration over nearly 40 km.

We choose hypocenters that can reasonably be assumed to be on or around the plate interface (Fig. 1(a)). This is based on the hypocentral depth distribution, which shows a tendency for the hypocenters to be localized to a plane of the presumed plate interface which, despite a certain limitation in the accuracy for these offshore events (Fig. 1(b), lower), is also strongly supported by the CMT solutions, manually determined by the National Research Institute for Earth Science and Disaster Prevention (available at www.fnet.bosai.go.jp), having nodal planes of low-angle reverse faulting (Fig. 1(c)). Note that such features become more obvious in our targeted area, located between the epicenters of the foreshock and mainshock, than in the case of further offshore events. The events of JMA magnitude larger than M_j 1 are included in Figs. 1(a) and (b) but events larger than M_j 2.6 are involved in the following quantitative analysis. To analyze background seismicity, we used the JMA earthquake catalog, and earthquakes smaller than M_j 6 are considered only after January 2000.

Because the propagation of slow slip induces stress perturbation on and around plate interfaces, we can expect the occurrence of earthquakes that are triggered by slow slip in the current sequence, as has been observed along the currently targeted subduction zone (e.g., Miyazaki *et al.*, 2004; Uchida *et al.*, 2004). This situation will also be similar to the generation of a non-volcanic tremor in association with slow slip events (SSEs) observed for the various plate interfaces (Rogers and Dragert, 2003; Obara *et al.*, 2004). Supported by these established observational facts, we can safely interpret the seismic activity change as the marker of the propagation of slow slip, i.e., after-slip.

3. Results

Figure 1(a) shows the spatio-temporal evolution of seismic activity during the two days between the foreshock and the mainshock. The colors of the epicenters denote the occurrence time of each earthquake so that we can trace temporal changes in the activity. As seen in the gradual changes of the colors, the seismicity migrated and expanded from the focal area of the foreshock, whilst there was an absence of seismicity in some areas. Finally, we can note that the migration reached the hypocentral location of the mainshock.

In this migration pattern, the speed of migration appears to decrease the further it goes. This deceleration might be related to a diffusional propagation of slow slip as considered in the above-mentioned studies. Therefore, we test this hypothesis by examining if the migration is explained by a parabolic curve fitting with a certain diffusion coefficient. For this purpose, we select two representative cross-sections A–A′ and B–B′ indicated by gray rectangles (Fig. 1(a)), which cover the area inbetween the foreshock and the mainshock. Because we want to follow how the mi-

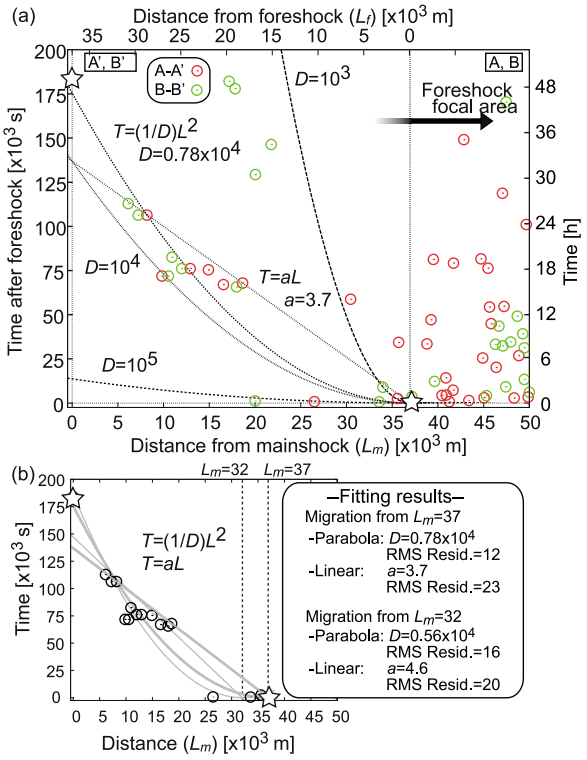

Fig. 2. Space-time plots of seismicity in the area between the foreshock and the mainshock. (a) Red and green open circles denote earthquake events plotted as functions of the elapsed time and the distance from the mainshock epicenter along the cross-sections A–A′ and B–B′, respectively (see Fig. 1(a)). Stars indicate hypocenters of the foreshock and the mainshock. Specification of fitting curves and line are indicated in the panel. (b) Black circles denote events taken from (a) to define the migration front and used for the least-squares analysis. Gray parabolic curves and lines show the resulting least-squares solutions specified in the inset; thick and thin curves are those from $L_{\rm m} = 37$ and $L_{\rm m} = 32$.

gration approaches the mainshock hypocenter, these cross-sections are chosen to radiate from this point. Then, we compare the data with the calculated migration distance L represented as the function of time T written as

$$L = (DT)^{1/2}. \tag{2}$$

First, we investigate the migration pattern on the map view (Fig. 1(a)). The colored tick marks appended inside the gray rectangles show the locations of the migration fronts at 6 hour intervals calculated from Eq. (2) assuming $D = 0.78 \times 10^4$ m^2 s^{-1} where the color coding corresponds to time after the foreshock (see color bar scale); these intervals become closer as time passes following Eq. (2). In this figure, it is immediately found that the calculated total migration distance bridges a gap between the foreshock focal area and the mainshock epicenter, meaning that the given value of D describes the overall rate of migration well. Comparisons between the colors of the ticks and the epicenters enable a more detailed investigation into the migration process. (Note that we need to trace the front of the migration, which corresponds to the first event at a certain location, whereas some events can be obscured by neighboring later events on this figure.) Although the event locations are spotty, we can see that the overall pattern of their gradual color changes is also well correlated with the tick colors. In particular, it is clearly seen that the migration front extended more than half the total distance during the first half a day, and took another 1.5 days to extend the remaining distance.

Next, in Fig. 2, we will detail the migration pattern on a space-time plot, which enables a more precise comparison of observation with theory. The occurrence time of the earthquakes included in the cross-sections A–A′ and B–B′ are plotted as a function of the epicentral distances. By observing Fig. 2(a), it is confirmed that the seismicity actually migrates from the foreshock focal area and then gradually approaches the mainshock hypocenter. Aside from the migration, the continuing activity around the foreshock hypocenter must be attributable to its aftershocks in the usual sense. Plotting Eq. (1) with $D = 0.78 \times 10^4$ placed the origin at the foreshock hypocenter, $L_{\rm m} \sim 37$, which actually is one of the least-squares solutions of the parabolic fitting described below, and we can see that the curve describes the trend of the migration front originating from there. Whilst the sole outlier is found near $L_{\rm m} = 20$ for the cross-section B–B′ and occurred within 2000 s, this might be triggered by coseismic stress changes rather than a propagating slow slip, since this location appears to be susceptible to a small stress observing the continuing activity resulted in a cluster (see also Fig. 1). Note that we do not attempt to discuss precisely the values of D, however, it is obvious that the values are in a range of an order of magnitude since $D = 10^3$ and 10^5 do not fit the data at all.

Finally, we quantitatively evaluate the other possibilities: (1) linear function fitting and (2) a different migration start point assumed at $L_{\rm m} = 32$ as an extreme case considering an extraordinarily larger foreshock focal area. Figure 2(b) shows the used dataset and the obtained least-squares solutions with the root mean squares of the sum of their squared residuals. In order that the dataset on the migration is kept as simple as possible, we eliminated only the obvious aftershocks and the above-mentioned continual activity, so as not to be biased too much by these different phenomena. As a result, we can see that the linear function fittings have larger residuals than the parabolic cases for both assumed starting points (Removing a tricky data point at $L_{\rm m} = 26$ changes the residual by less than 10%, and does not change this tendency.) Moreover, we find that the linear cases cannot follow the overall trend if one attempts to explain reasonably all the data points from the foreshock area, $L_{\rm m} \sim 37$, to the mainshock hypocenter, $L_{\rm m} = 0$, through the recognizable migration front between $L_{\rm m} \sim 5$–20 (the reason for the lack of seismicity inbetween is discussed below). These fitting results are basically valid even allowing for possible epicentral determination errors.

4. Discussions and Conclusion

Here, we will overview the seismic background of this region (Fig. 3). This region is rich in seismic activity often becoming M 5-class but occasionally M 7-class. As shown in Fig. 3(a), such relatively large events appear to be concentrated on the western, down-dip, half of this region, overlapped with clouds of background seismicity. There was a sequence in January 1981 involving events of $M_{\rm j}$ 6.0–7.0 in and around the focal area of the current foreshock. In Fig. 3(b), it is also shown that the foreshock area extends

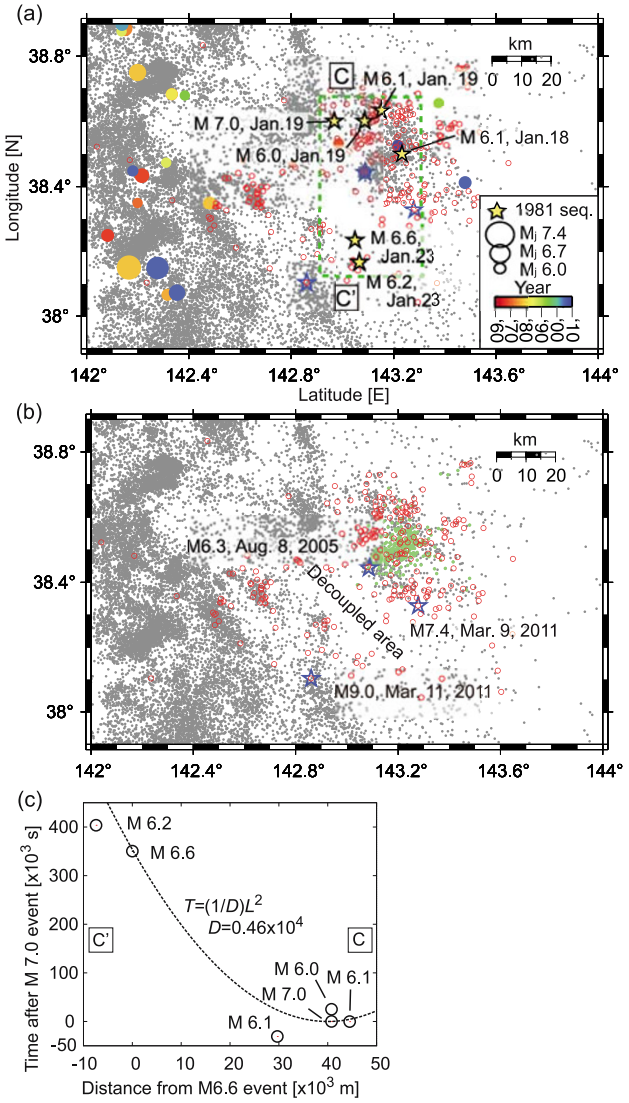

Fig. 3. Spatial distribution of background seismicity. (a) Filled circles denote events larger than M_j 6 which occurred from 1967 to 2010 (see inset for magnitudes and origin times, respectively, depicted by sizes and colors). Open red circles denote seismicity in the current foreshock-mainshock sequence. Gray dots denote the seismicities of the background in the time and depth ranges of January 2000—September 2010 and 1–50 km, respectively. Blue stars denote epicenters of the current foreshock and mainshock, and the 2005, M_j 6.3, event as indicated in (b). (b) Green dots denote seismicity activated in August 2005. (c) Space-time plot of seismic sequence of 1981 along the rectangular cross-section C–C′ shown in (a).

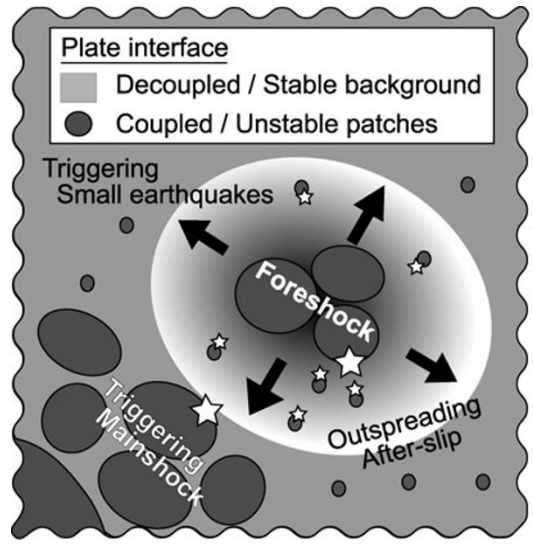

Fig. 4. Schematic diagram showing an earthquake sequence on the plate interface from the foreshock to the mainshock. White stars illustrate hypocenters. Weak planes located around the plate interface (not shown here) can be ruptured during the sequence.

over a cluster, which was activated with M_j 6.3, on August 24, 2005. In addition, the after-slip-induced activities (see Figs. 1 and 3) overlap with obvious clusters observed in the background seismicity. It is important to point out that the focal areas of the current events obviously correlate with these previous focal areas which suggests the existence of persistent fault structures, but the rupture processes are not just repetitions having the same form.

In Fig. 2, we saw an area with an apparent lack of seismicity for $L_m \sim 20$–35. This apparent deficit seems to be characteristic of this area as exemplified by long-term seismic activity (Fig. 3). We can, perhaps, suppose both decoupling and coupling just to interpret this seismic gap but the slow propagation of the after-slip through the gap is incompatible with the latter because, if such a large coupled patch breaks, the rupture would be accelerated to be a standard earthquake. Therefore we can presume that this area is persistently decoupled as indicated in Fig. 3(b). In this respect, the seismic sequence in January, 1981, provides an interesting perspective because, beyond this gap, the onset of the M 6.6 events on January 23 was largely delayed after the M 7.0 event on January 19. In fact, it suggests that the delay can be explained by a parabolic curve with $D = 0.46 \times 10^4$ (Fig. 3(c)), which is the same, by an order of magnitude, as that for the current foreshock-mainshock sequence.

Although detailed physical interpretations are beyond the focus of this paper, it might be worth providing an illustration of possible rupture mechanisms and fault properties underlying this observed sequence (Fig. 4). It is considered that the foreshock broke through strongly-coupled neighboring patches existing on an otherwise decoupled background. The rupture initiated near the rim of a patch probably due to stress concentration by steady sliding on the surrounding stable area. The background is stable with a fault property exhibiting velocity strengthening, so that the raised stress along the perimeter of the broken area starts to slowly diffuse with after-slip; the velocity strengthening is essential to interpret the slow after-slip otherwise the after-slip ceases immediately transferred by a seismic wave. Distributed small coupled patches were overrun in the after-slip propagation and ruptured seismically, resulting in signals which indicated the location of the propagation front. The after-slip finally reached the location of the mainshock hypocenter and triggered the dynamic rupture there, presumably involving multiple patches. The active production and partitioned slip distribution of major ($M \geq 7$) interplate aftershocks (Kiser and Ishii, 2011) suggest the existence of such a heterogeneous fault structure. On the other hand, the after-slip alone could not have caused the gigantic earthquake because the stress perturbation accompanying

the after-slip did not have such a large reach, therefore it has to be considered that the coupled patches in the mainshock focal area were tectonically pre-stressed and susceptible to triggering by the after-slip and to sustaining the rupture propagation. Either way, the after-slip of the foreshock probably played a role of giving the last push.

The above view is qualitatively supported by physics-based simulations (Ando *et al*., 2010; Nakata *et al*., 2011) demonstrating that, if a number of coupled patches almost equally reach their critical stress state, these patches can be ruptured in a sequence even though the patches are sparsely distributed to some extent. We speculate that such a synchronization, which rarely occurs over a great distance, might have happened this time. The simulations further clarify that the degree of the patch interactions is controlled by the patch distributions, and that the parabolic and diffusional slow slip propagation occurs under a certain rheological fault condition.

The existence of a strict control in after-slip propagation (Eq. (2)) and the possibility of signal detection offer a chance to predict the occurrence of subsequent earthquakes in the preceding hours or days, although we may always expect fluctuations depending on conditions. However, because this phenomenon alone cannot alert us to earthquake generation, in order to accomplish such a prediction we need to know beforehand the locations of coupled patches and their tectonic stress levels. Such evaluations could be made possible by improvements in geodetic (e.g., Hashimoto *et al*., 2009) and seismic (e.g., Uchida *et al*., 2004) monitoring for plate coupling, combined with paleo-seismological history reconstruction (e.g., Sawai *et al*., 2009) to quantify elapsed times since previous earthquakes and their magnitudes. It is also essential to develop proper physical fault models to input these data and to translate them into physical fault states. Since the degree of plate-coupling has localities (Lay and Kanamori, 1981) and the interactive behaviors between fault segments (or patches) are not straightforward, a physics-based understanding is important to compensate for our limited experiences. Earthquake studies following such a direction could be applied to consider other potentially catastrophic earthquakes, such as that on the Nankai subduction zone off southwest Japan.

Acknowledgments. Suggestions by Y. Yoshida improved the manuscript. We are grateful to the Japan Meteorological Agency (JMA) for the P- and S-phase arrival time readings and the earthquake catalog. The data was processed in collaboration with the JMA and the Ministry of Education, Culture, Sports, Science and Technology (MEXT). This work was partially supported by MEXT KAKENHI (21107007).

References

Ando, R., R. Nakata, and T. Hori, A slip pulse model with fault heterogeneity for low-frequency earthquakes and tremor along plate interfaces, *Geophys. Res. Lett.*, **37**, doi: 10.1029/2010GL043056, 2010.

Engdahl, E. R., A. Villasenor, H. R. DeShon, and C. H. Thurber, Teleseismic relocation and assessment of seismicity (1918-2005) in the region of the 2004 M-w 9.0 Sumatra-Andaman and 2005 M-w 8.6 Nias Island great earthquakes, *Bull. Seismol. Soc. Am.*, **97**, S43–S61, 2007.

Gomberg, J., P. A. Reasenberg, P. Bodin, and R. A. Harris, Earthquake triggering by seismic waves following the Landers and Hector Mine earthquakes, *Nature*, **411**, 462–466, 2001.

Hashimoto, C., A. Noda, T. Sagiya, and M. Matsu'ura, Interplate seismogenic zones along the Kuril-Japan trench inferred from GPS data inversion, *Nature Geosci.*, **2**, 141–144, 2009.

Hayes, G., Finite fault model, preliminary result of the Mar 9, 2011 Mw 7.2 Earthquake Offshore Honshu, Japan, http://earthquake.usgs.gov/earthquakes/eqinthenews/2011/usb0001r57/finite_fault.php, Last accessed 4/1/2011.

Ida, Y., Slow-moving deformation pulses along tectonic faults, *Phys. Earth Planet. Inter.*, **9**, 328–337, 1974.

Ide, S., Striations, duration, migration and tidal response in deep tremor, *Nature*, **466**, 356-U105, 2010.

Ide, S., G. C. Beroza, D. R. Shelly, and T. Uchide, A scaling law for slow earthquakes, *Nature*, **447**, 76–79, 2007.

King, G. C. P., R. S. Stein, and J. Lin, Static stress changes and the triggering of earthquakes, *Bull. Seismol. Soc. Am.*, **84**, 935–953, 1994.

Kiser, E. and M. Ishii, Preliminary rupture modelling of the March 11, 2011 Tohoku-Chiho Taiheiyo-Oki Earthquake and sequence of events using the USArray transportable array, http://www.seismology.harvard.edu/research_japan.html, Last accessed 4/1/2011.

Lay, T. and H. Kanamori, Earthquake doublets in the Solomon-Islands, *Phys. Earth Planet. Inter.*, **21**, 283–304, 1980.

Lay, T. and H. Kanamori, An asperity model of great earthquake sequences, in *Earthquake Prediction—An International Review*, AGU Geophys. Mono., edited by D. W. Simpson and P. G. Richards, pp. 579–592, AGU, Washington, D.C., 1981.

Lehner, F. K., V. C. Li, and J. R. Rice, Stress diffusion alongr rupturing plate boundaries, *J. Geophys. Res.*, **86**, 6155–6169, 1981.

Miyazaki, S., P. Segall, J. Fukuda, and T. Kato, Space time distribution of afterslip following the 2003 Tokachi-oki earthquake: Implications for variations in fault zone frictional properties, *Geophys. Res. Lett.*, **31**, doi:10.1029/2004GL021457, 2004.

Nakano, M., H. Kumagai, S. Toda, R. Ando, T. Yamashina, H. Inoue, and Sunarjo, Source model of an earthquake doublet that occurred in a pull-apart basin along the Sumatran fault, Indonesia, *Geophys. J. Int.*, **181**, 141–153, 2010.

Nakata, R., R. Ando, T. Hori, and S. Ide, Generation mechanism of slow earthquakes: Numerical analysis based on a dynamic model with brittle-ductile mixed fault heterogeneities, *J. Geophys. Res.*, 2011 (in press).

Obara, K., H. Hirose, F. Yamamizu, and K. Kasahara, Episodic slow slip events accompanied by non-volcanic tremors in southwest Japan subduction zone, *Geophys. Res. Lett.*, **31**, doi:10.1029/2004GL020848, 2004.

Rogers, G. and H. Dragert, Episodic tremor and slip on the Cascadia subduction zone: The chatter of silent slip, *Science*, **300**, 1942–1943, 2003.

Savage, J. C., A theory of creep waves propagating along a transform fault, *J. Geophys. Res.*, **76**, 1954–1966, 1971.

Sawai, Y., T. Kamataki, M. Shishikura, H. Nasu, Y. Okamura, K. Satake, K. H. Thomson, D. Matsumoto, Y. Fujii, J. Komatsubara, and T. T. Aung, Aperiodic recurrence of geologically recorded tsunamis during the past 5500 years in eastern Hokkaido, Japan, *J. Geophys. Res.*, **114**, 10.1029/2007JB005503, 2009.

Uchida, N., A. Hasegawa, T. Matsuzawa, and T. Igarashi, Pre- and post-seismic slow slip on the plate boundary off Sanriku, NE Japan associated with three interplate earthquakes as estimated from small repeating earthquake data, *Tectonophysics*, **385**, 1–15, 2004.

Waldhauser, F. and W. L. Ellsworth, A double-difference earthquake location algorithm: Method and application to the northern Hayward fault, California, *Bull. Seismol. Soc. Am.*, **90**, 1353–1368, 2000.

Yagi, Y. J. and M. Kikuchi, Partitioning between seismogenic and aseismic slip as highlighted from slow slip events in Hyuga-nada, Japan, *Geophys. Res. Lett.*, **30**, 2003.

R. Ando (e-mail: ryo-ando@aist.go.jp) and K. Imanishi